

Matrix Normal PCA for Interpretable Dimension Reduction and Graphical Noise Modeling

Chihao Zhang, Kuo Gai and Shihua Zhang

Abstract—Principal component analysis (PCA) is one of the most widely used dimension reduction and multivariate statistical techniques. From a probabilistic perspective, PCA seeks a low-dimensional representation of data in the presence of independent identical Gaussian noise. Probabilistic PCA (PPCA) and its variants have been extensively studied for decades. Most of them assume the underlying noise follows a certain independent identical distribution. However, the noise in the real world is usually complicated and structured. To address this challenge, some non-linear variants of PPCA have been proposed. But those methods are generally difficult to interpret. To this end, we propose a powerful and intuitive PCA method (MN-PCA) through modeling the graphical noise by the matrix normal distribution, which enables us to explore the structure of noise in both the feature space and the sample space. MN-PCA obtains a low-rank representation of data and the structure of noise simultaneously. And it can be explained as approximating data over the generalized Mahalanobis distance. We develop two algorithms to solve this model: one maximizes the regularized likelihood, the other exploits the Wasserstein distance, which is more robust. Extensive experiments on various data demonstrate their effectiveness.

Index Terms—Principal component analysis, dimension reduction, matrix normal distribution, sparse inverse covariance, graphical noise modeling



1 INTRODUCTION

HIGH-DIMENSIONAL data emerge from diverse fields of science and engineering dramatically. For example, biologists can use microarray to detect the expression of thousands of genes at the same time; a single picture consists of hundreds, thousands, or even more pixels. Generally, those data are redundant and noisy. Directly extracting useful information from the primitive data is often infeasible. Therefore, how to discover the compact and meaningful representation of high-dimensional data becomes a fundamental problem. Researchers have developed many powerful methods to address this problem from different perspectives. Among those methods, principal component analysis (PCA) is one of the most fundamental and widely used data mining and multivariate statistical techniques. Since Pearson [1] invented it in 1901, PCA has become a standard approach for dimension reduction and feature extraction, and has numerous applications in various fields, such as signal processing [2], human face recognition [3] and gene expression analysis [4].

PCA obtains a low-dimensional representation for high-dimensional data in a L_2 sense. However, it is known that PCA is sensitive to gross errors. To remove the effect of sparse gross errors, robust PCA (RPCA) [5], [6], [7] has been proposed. Specifically, RPCA seeks to decompose the data matrix as a superposition of a low-rank matrix with a sparse matrix. The sparse matrix captures the gross errors and enables RPCA to recover the underlying low-rank representation of the primitive data accurately. RPCA has been

demonstrated to have a number of applications in various fields [7], [8], [9], [10].

To tackle the noise of data implicitly, regularized methods have been introduced. A common assumption is that if two data points are close in the original space, their representations should be close to each other too. To preserve the local geometrical structure in the representation, graph regularizers are imposed. Gao *et al.* [11] proposed a sparse coding method which exploits the dependence among the feature space by constructing a Laplace matrix. Zheng *et al.* [12] also proposed a graph regularized sparse coding to learn the sparse representations that explicitly takes into account the local manifold structure of the data. More recently, Yin *et al.* [13] proposed a low-rank representation method that considers the geometrical structure in both the feature space and the sample space. As many measurements in experiments are naturally nonnegative, there are also some nonnegative matrix factorization variants with graph regularization [14], [15].

Probabilistic approaches are natural ways to account for different types of noise in data. Tipping and Bishop [16] first introduced a probabilistic PCA (PPCA) method, and showed that PCA could be derived from a Gaussian latent variable model. PPCA assumes that the underlying distribution of noise is independent and identical Gaussian distribution (IID), and the maximum likelihood estimation leads to a PCA solution. This probabilistic framework allows various extensions of PCA. For example, Bishop extended PCA by a Bayesian method [17] (BPCA) and showed that the number of retained principal components could be determined automatically as part of the Bayesian inference procedure. To handle different types of errors, researchers have also introduced different distributions. Zhao and Jiang [18] used the multivariate Student's t distribution to model the noise (tPPCA). Their experiments show that tPPCA requires

• Chihao Zhang, Kuo Gai and Shihua Zhang* are with the NCMIS, CEMS, RCSDS, Academy of Mathematics and Systems Science, Chinese Academy of Sciences, Beijing 100190, China, and School of Mathematical Sciences, University of Chinese Academy of Sciences, Beijing 100049, China.

*To whom correspondence should be addressed. Email: zsh@amss.ac.cn.

a smaller model size and has better performance than PPCA. Wang *et al.* [19] introduced the Laplace distribution to model the noise (RPMF), which is more robust to outliers. Li and Tao [20] employed the exponential family distributions to handle general types of noise. Most of those variants assume the underlying distribution of noise is IID.

However, the noise in the real-world is usually complicated and structured. The IID assumption no longer holds. For example, the noise of gene expression may demonstrate different patterns under different biological conditions or techniques. Data collected from different sources may contain heterogeneous noise. Zhang and Zhang [21] developed a Bayesian joint matrix decomposition method (BJMD) to model the heterogeneous noise of multi-view data by the Gaussian distribution. Zhao *et al.* [22] introduced the mixture of the Gaussian noise to model the complex noise and Cao *et al.* further generalized this model to the mixture of the exponential family noise [23]. Those methods assume the noises are generated by different distributions, but the independent assumption still holds. Beyond the independent assumption, Kalaitzis and Lawrence [24] generalized PPCA by adding a fixed random effect (RCA) to decompose the residual variance. RCA can be interpreted as the IID Gaussian noise with a linear offset in the feature space. Some researchers also adopted kernel methods to handle the non-linear noise [25], [26], [27]. However, those non-linear methods are often difficult to interpret.

To this end, we propose a powerful and intuitive PCA model (MN-PCA) to obtain the low-rank representation and the structure of the underlying noise simultaneously. Specifically, we use a matrix normal distribution to model the correlated noise. The inference of the precision matrices of the matrix normal distribution turns to be that of two Gaussian graphical models, enabling us to explore the structure of the noise in both the feature space and the sample space. We develop two algorithms to solve this model: one is to maximize the regularized likelihood function directly; the other is to minimize the discrepancy between the distribution of the white matrix normal and that of the residue. We extensively compare the two algorithms and discuss their advantages and disadvantages. Extensive experiments on various data show their effectiveness. By considering the structure of the underlying noise, MN-PCA generally obtains a better low-rank representation, and the inferred structure of the noise reveals some interesting information that is ignored by other methods.

2 RELATED WORK

2.1 PCA

There are two common formulations of PCA that give rise to the same algorithm [28]. From a dimension reduction perspective, PCA seeks a low-dimensional sub-space in which the projected variance of the data is maximized. Specifically, let $Y \in R^{n \times p}$ be the data matrix of n observations and p variables. For simplicity, assume the data matrix Y is already centered. The first principal component is defined as $z_1 = \sum_{j=1}^p v_{1j} X_{.j}$, where the vector $v_1 = (v_{11}, \dots, v_{1p})^T$ is chosen to maximize the variance of z_1 , i.e.,

$$v_1 = \arg \max_v v^T S v \quad \text{subject to } \|v\| = 1, \quad (1)$$

where $S = Y^T Y / n$ is the $p \times p$ covariance matrix. The next principal components v_{k+1} are defined in sequence:

$$v_{k+1} = \arg \max_v v^T S v, \quad (2)$$

subject to $\|v\| = 1, v^T v_l = 0, \forall 1 \leq l \leq k$.

This definition implies that the first K principal components are the first K eigenvectors of S . Thus, we can use the singular value decomposition (SVD) to perform PCA. Let the SVD of Y be

$$Y = U \Sigma V^T, \quad (3)$$

where $U \in R^{n \times p}$ and $V \in R^{p \times p}$ are orthogonal matrix, $\Sigma \in R^{p \times p}$ is a diagonal matrix with the diagonal elements σ_i in descending order. By $XV = U\Sigma$, we see that $z_k = U_{.k} \sigma_k$.

PCA can also be interpreted as minimizing the reconstruction error. Given Y , we aim at finding a low-rank approximation of $Y \approx XW^T$ under the Frobenius norm:

$$\min \|Y - XW^T\|_F^2, \quad (4)$$

where $X \in R^{n \times r}$ and $W \in R^{p \times r}$. Eckart and Young [29] showed that truncated SVD has the optimality property:

$$\|Y - Y_r\|_F \leq \|Y - B\|_F \quad (5)$$

where $Y_r = U_r \Sigma_r V_r^T$ is the truncated SVD of Y , and B is any matrix of rank at most r . Thus, Y_r is the best rank- k approximation of Y under the Frobenius norm. Then $X = U_r \Sigma_r$ is the PC scores, $W = V_r$ is the principal directions, and $XW^T = Y_r$.

2.2 Robust PCA

PCA is sensitive to outliers. RPCA has been proposed to improve it. Specifically, RPCA seeks to decompose the data matrix Y into two parts:

$$Y = L + S, \quad (6)$$

where L is a low-rank matrix and S is a sparse matrix. The gross errors will be captured by the sparse matrix S and the low-rank matrix L can still approximate Y well. Mathematically, the objective function of RPCA can be written as:

$$\min_{L, S} \|L\|_* + \rho \|S\|_1 \quad \text{s.t. } L + S = Y, \quad (7)$$

where $\|L\|_*$ is called the nuclear norm of L which is the sum of the singular values of L . The nuclear norm is a convex relaxation of rank norm. $\|S\|_1$ encourages the sparsity of S . However, algorithms dealing with the nuclear norm usually involve computing SVD, which is very time consuming when the problem size is large. To avoid the SVD, one way is to factorize the low-rank matrix L as a product of two low-rank matrices, i.e., $L = XW^T$, where $X \in R^{n \times r}$, $W \in R^{p \times r}$, and $r \ll \min(m, n)$. For example, Zhou and Tao [30] formulated a regularized RPCA as follows:

$$\min_{X, W, S} \left\| Y - (S + XW^T) \right\|_F^2 + \rho \|S\|_1 \quad (8)$$

with some low-rank constraints on X and W . The Frobenius term indicates the goodness of approximation. The authors show that the problem can be solved efficiently by a block alternating minimization algorithm. Readers may refer to [31] for the recent advances about RPCA.

2.3 Graph Regularized Matrix Factorization

Graph regularized matrix factorization methods obtain the low-rank representation of the primitive data and somehow preserve the local geometry structure by graph regularizers. For example, Zheng *et al.* [12] proposed a graph regularized sparse coding method for image presentation:

$$\min \left\| Y - XW^T \right\|_F^2 + \eta \operatorname{tr}(X^T L X) + \rho \|X\|_1, \quad (9)$$

where $\eta > 0$, $\rho > 0$. X is the sparse low-dimensional representation of images. $L \in R^{n \times n}$ is the Laplacian matrix of a graph. We can construct a binary graph matrix G by the k -NN approach:

$$G_{ij} = \begin{cases} 1, & \text{if } x_i \text{ is a neighbor of } x_j \\ 0, & \text{otherwise.} \end{cases} \quad (10)$$

Given the degree matrix $D = \operatorname{diag}(d_1, \dots, d_n)$, where $d_i = \sum_{j=1}^n G_{ij}$, the Laplacian matrix is defined as $L = D - G$. Note that the graph regularizers can be written as

$$\operatorname{tr}(X^T L X) = \frac{1}{2} \sum_{ij} (x_i - x_j)^2 G_{ij}. \quad (11)$$

Therefore, the graph regularizer $\operatorname{tr}(X^T L X)$ encourages samples that are close in the original space to be neighbors in the sparse representation X . Moreover, Yankelevsky and Elad [32] proposed a low-rank representation method, which considers the geometry structure in both the feature and sample spaces:

$$\begin{aligned} \min_{X, W} & \left\| Y - XW^T \right\|_F^2 + \eta_1 \operatorname{tr}(X^T L_1 X) + \eta_2 \operatorname{tr}(W^T L_2 W) \\ \text{s.t.} & \|x_i\|_0 \leq T \quad \forall i, \end{aligned} \quad (12)$$

where L_1 and L_2 are the Laplacian matrices in both spaces, respectively. $T > 0$ controls the sparsity of x_i .

2.4 Probabilistic PCA and its variants

Tipping and Bishop [16] showed that PCA could be derived from a Gaussian latent variable (named as Probabilistic PCA, or PPCA). The generative model of PPCA is:

$$Y = XW^T + E, \quad (13)$$

where $X \in R^{n \times r}$, $W \in R^{p \times r}$ and $E_{ij} \stackrel{IID}{\sim} \mathcal{N}(0, \sigma^2)$. The negative log-likelihood is as follows:

$$\frac{1}{2\sigma^2} \left\| Y - XW^T \right\|_F^2 + np \log \sigma. \quad (14)$$

PPCA conventionally defines standard Gaussian $\mathcal{N}(0, I)$ prior on each column of X and derive the maximum likelihood estimation (MLE) of W and σ .

The goal of PPCA is not to give better results than PCA, but to permit a broad range of future extensions by facilitating various probabilistic techniques and introducing different assumptions of distribution. For example, Bishop [33] developed a variational formulation of Bayesian PCA, which can automatically determine the number of retained principal components; Zhao and Jiang [18] proposed tPPCA which assumes that data are sampled from multivariate

Student- t distribution; Wang *et al.* [19] formulated a probabilistic robust matrix factorization (RPMF) by introducing the Laplace distribution over E , which is more robust to outliers. Note that most of those methods assume that the underlying distribution of data are IID.

To allow the model to account for general types of noise, Zhao *et al.* [22] relaxed the IID assumption and introduced the mixture of Gaussian noise to model the complex noise. Cao *et al.* further extended the model to the mixture of exponential family noise [23]. Note that such noise is not identical but still independent. Inspired by the linear mixed model, Kalaitzis and Lawrence [24] proposed RCA to generalize PPCA by adding fixed effects onto Eq. (13), i.e.

$$Y = XW^T + ZV^T + E, \quad (15)$$

where Z is a matrix of known covariates. The loading matrices W and V can be marginalized with the Gaussian isotropic priors

$$\ln p(Y) \sum_{j=1}^n \ln \mathcal{N}(Y_{\cdot j} | 0, X X^T + \Sigma), \quad (16)$$

where $\Sigma = Z Z^T + \sigma^2 I$. Σ can be interpreted as an offset of the covariance on the feature space. To utilize the covariances in both the sample and feature spaces, Allen *et al* [34] proposed a generalized PCA (GPCA)

$$\begin{aligned} \max_{v_k} & v_k^T \Sigma^{-1} Y^T \Omega^{-1} Y \Sigma^{-1} v_k \\ \text{s.t.} & v_k^T \Sigma^{-1} v_k = 1 \text{ and } v_k^T \Sigma^{-1} v_{k'} = 0 \quad \forall k' < k, \end{aligned} \quad (17)$$

where Ω^{-1} and Σ^{-1} are predefined $n \times n$ and $p \times p$ positive semi-definite matrices based on prior knowledge, respectively. Ω^{-1} and Σ^{-1} are the precision matrices in the sample and feature spaces respectively.

To handle the nonlinearity, some authors extended PPCA inspired by the kernel methods [35], [36], [37]. Moreover, Lawrence [27] introduced an alternative probabilistic interpretation of PPCA (named as dual PPCA, or DPPCA) and non-linear DPPCA through Gaussian processes. But those non-linear methods are often difficult to explain.

2.5 Gaussian Graphical Model

Gaussian graphical models (GGM) have been proposed to understand the statistical relationship between variables of interest in the form of a graph. Specifically, those models use multivariate Gaussian distribution to model the statistical relationship between variables. The precision matrix of the multivariate Gaussian reveals the conditional correlations between pairs of variables. How to estimate a large precision matrix is fundamental in modern multivariate analysis. Formally, suppose one has n multivariate normal observations of dimension p with covariance Σ . Let $\Theta = \Sigma^{-1}$ be the precision matrix, and S be the empirical covariance matrix; then the problem is to maximize the log-likelihood:

$$\log \det \Theta - \operatorname{tr} S \Theta. \quad (18)$$

To estimate a large precision matrix, the sparse assumption is made in literature, i.e., many entries in the precision matrix Θ are zeros. Thus, one can add the L_1 -penalty onto the log-likelihood:

$$\log \det \Theta - \operatorname{tr} S \Theta - \rho \|\Theta\|_1, \quad (19)$$

where Θ is positive definite, and $\rho > 0$ controls the sparsity of Θ . This problem has been extensively studied [38], [39], [40], [41], [42], [43]. Readers may refer to [44] for a comprehensive review.

3 MATRIX NORMAL PCA

3.1 Model Construction

Most probabilistic methods assume the underlying noise E is IID. Though the IID assumption enjoys good theoretical properties, it is easily violated in real-world data. To model the underlying correlated noise (graphical noise), a naive approach is to assume that the noise follows a multivariate Gaussian distribution, i.e., $E \sim \mathcal{N}(\text{vec}(E), \Sigma)$. However, E consists of np variables, the corresponding covariance matrix Σ is of size $np \times np$ which is too huge and thus infeasible.

Instead, we assume that the noise is correlated in both the sample and feature spaces. We use a matrix normal distribution to model the among-sample and among-feature covariance of noise simultaneously. Due to its close relationship with PCA, we name it as MN-PCA (Fig. 1). Specifically, MN-PCA follows the similar generative model as PPCA

$$Y = XW^T + E. \quad (20)$$

But MN-PCA assumes $E \sim \mathcal{MN}_{n,p}(0, \Omega, \Sigma)$, where $\Omega_{n \times n}$ and $\Sigma_{p \times p}$ are among-row and among-column variance respectively. Note that the matrix normal is related to the multivariate normal distribution in the following way:

$$E \sim \mathcal{MN}_{n,p}(M, \Omega, \Sigma), \quad (21)$$

if and only if

$$\text{vec}(E) \sim \mathcal{N}_{np}(\text{vec}(M), \Omega \otimes \Sigma), \quad (22)$$

where \otimes denotes the Kronecker product. Therefore, the density function of $\mathcal{MN}_{n,p}(M, \Omega, \Sigma)$ has the form:

$$P(Y|M, \Omega, \Sigma) = \frac{\exp\left[-\frac{1}{2} \text{tr}\left(\Sigma^{-1}(Y - M)^T \Omega^{-1}(Y - M)\right)\right]}{(2\pi)^{\frac{np}{2}} |\Omega|^{\frac{n}{2}} |\Sigma|^{\frac{p}{2}}}. \quad (23)$$

Accordingly, the negative log-likelihood of MN-PCA is

$$\begin{aligned} \mathcal{L} = & \frac{1}{2} \text{tr}\left[\Sigma^{-1}(Y - XW^T)^T \Omega^{-1}(Y - XW^T)\right] \\ & + \frac{p}{2} \log |\Omega| + \frac{n}{2} \log |\Sigma|. \end{aligned} \quad (24)$$

Now we successfully reduce the number of parameters of the covariance from $n^2 p^2$ to $n^2 + p^2$, but it is still infeasible to minimize the negative log-likelihood in Eq. (24). That is because the number of free parameters in Ω and Σ grows quadratically with n and p , respectively. To address this issue, we impose sparse constraints on the precision matrices Ω^{-1} and Σ^{-1} by introducing the L_1 regularization terms:

$$\begin{aligned} \mathcal{L} = & \frac{1}{2} \text{tr}\left[\Sigma^{-1}(Y - XW^T)^T \Omega^{-1}(Y - XW^T)\right] \\ & + \frac{p}{2} \log |\Omega| + \frac{n}{2} \log |\Sigma| + n\lambda_1 \|\Omega^{-1}\|_1 + p\lambda_2 \|\Sigma^{-1}\|_1, \end{aligned} \quad (25)$$

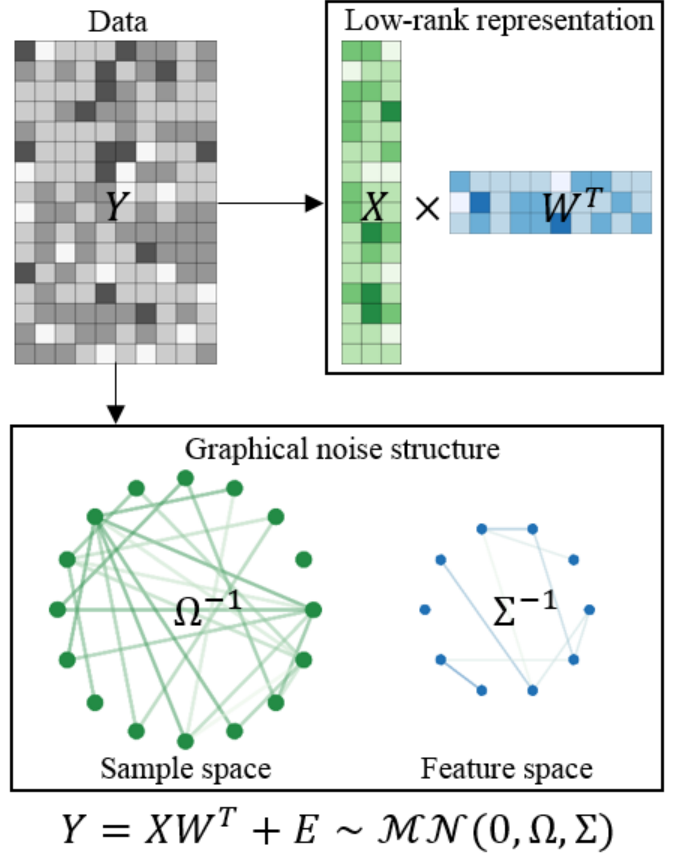


Fig. 1. Illustration of MN-PCA. MN-PCA models the low-rank representation and the structure of noise in both feature and sample spaces.

where λ_1, λ_2 control the sparsity of Ω^{-1} and Σ^{-1} , respectively. Note that Ω and Σ are positive-definite. We can further rewrite Eq. (25) in the Frobenius norm:

$$\begin{aligned} \mathcal{L} = & \frac{1}{2} \left\| \Omega^{-\frac{1}{2}}(Y - XW^T) \Sigma^{-\frac{1}{2}} \right\|_F^2 + \frac{n}{2} \log |\Omega| + \frac{p}{2} \log |\Sigma| \\ & + n\lambda_1 \|\Omega^{-1}\|_1 + p\lambda_2 \|\Sigma^{-1}\|_1. \end{aligned} \quad (26)$$

Let Ω and Σ be identity matrix, then \mathcal{L} reduces to

$$\mathcal{L} = \frac{1}{2} \left\| Y - XW^T \right\|_F^2. \quad (27)$$

Therefore, minimizing the reconstruction error in the Frobenius norm is a special case under the matrix normal assumption. MN-PCA degenerates to the classical PCA when Ω and Σ are identity matrices.

3.2 Model Interpretation

Intuitively, PCA can be interpreted as finding a linear manifold that minimizes the projection errors. Specifically, we rewrite the minimizing reconstruction errors form Eq. (4) of PCA as follows:

$$\min \sum_{i=1}^n (y_i - x_i W^T)(y_i - x_i W^T)^T, \quad (28)$$

where the summation terms are the Euclidean distance between sample vectors and the reconstruction vectors.

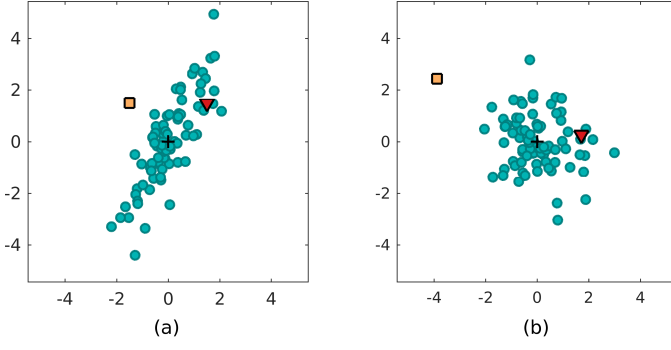


Fig. 2. Illustration of the Mahalanobis distance in a 2D data. The blue dots are drawn from a 2D Gaussian distribution. The cross mark indicates the center of the distribution.

However, computing Euclidean distance directly can be problematic.

For example, we want to measure the distance between a point x and a two-dimensional (2D) multivariate Gaussian $\mathcal{N}(\mu, \Sigma)$. The Euclidean distance $(x - \mu)^T(x - \mu)$ is a direct choice. As shown in Fig. 2(a), the Euclidean distance between the square and triangle points to the distribution centroid (cross mark) are equal. But the density of the multivariate Gaussian near the square point is smaller than that near the triangle point. Therefore, The square point to the center distance is intuitively farther than the triangle point. Mahalanobis distance is a proper measure for this situation:

$$d(x, \mu) = (x - \mu)^T \Sigma^{-1} (x - \mu). \quad (29)$$

We transform the covariance of the multivariate Gaussian to the identity matrix by a linear transformation. Then the Mahalanobis distance is computed by the Euclidean distance in the transformed space. Fig. 2(b) shows that after the transformation, the square point is farther from the centroid in term of the Euclidean distance. MN-PCA can be regarded as minimizing the reconstruction errors over the generalized Mahalanobis distance. When the covariance in sample space is an identity matrix, i.e., $\Omega = I$, the reconstruction error of MN-PCA can be written as:

$$\min \sum_{i=1}^n (y_i - x_i W^T) \Sigma^{-1} (y_i - x_i W^T)^T. \quad (30)$$

Note that Σ is the covariance matrix in the feature space. Thus the terms in summation are exactly the Mahalanobis distance. When Σ is an identity matrix, it is also a Mahalanobis distance:

$$\min \sum_{j=1}^p (y_{\cdot j} - X w_j^T) \Omega^{-1} (y_{\cdot j} - X w_j^T)^T. \quad (31)$$

Thus, we can regard MN-PCA as a minimization of the reconstruction error over the generalized Mahalanobis distance.

3.3 Maximum Regularized Likelihood

Here we present an alternatively iterative update procedure to seek the maximum regularized likelihood (MRL):

$$\begin{aligned} \min \mathcal{L} &= \frac{1}{2} \text{tr} \left[\Sigma^{-1} (Y - XW^T)^T \Omega^{-1} (Y - XW^T) \right] \\ &\quad + \frac{p}{2} \log |\Omega| + \frac{n}{2} \log |\Sigma| + n\lambda_1 \|\Omega^{-1}\|_1 + p\lambda_2 \|\Sigma^{-1}\|_1 \\ \text{s.t. } \Omega &\in S_{++}^n, \Sigma \in S_{++}^p, \end{aligned} \quad (32)$$

where $\Omega \in S_{++}^n$ denotes that Ω is a $n \times n$ symmetric positive definite matrix. This is a matrix optimization problem involving four matrix variables X , W , Ω and Σ . We adopt a block coordinate descent strategy to minimize \mathcal{L} .

Updating X and W : Retain the terms involving X and W

$$\min \mathcal{L} = \frac{1}{2} \left\| \Omega^{-\frac{1}{2}} Y \Sigma^{-\frac{1}{2}} - \Omega^{-\frac{1}{2}} X W^T \Sigma^{-\frac{1}{2}} \right\|_F^2 \quad (33)$$

Let Y' be $\Omega^{-\frac{1}{2}} Y \Sigma^{-\frac{1}{2}}$. By Eckart and Young's theorem, the best rank- k approximation of Y' in the Frobenius norm is the truncated k SVD of Y' , i.e. $Y'_r = U_r \Sigma_r V_r^T$. Let

$$X = \Omega^{\frac{1}{2}} U_r \Sigma_r, \quad W = \Sigma^{\frac{1}{2}} V_r. \quad (34)$$

Then $\Omega^{-\frac{1}{2}} X W^T \Sigma^{-\frac{1}{2}} = Y'_r$ and the objective function is minimized. Thus we obtain the closed-form solution of X and W for Eq. (33). However, computing $\Omega^{-\frac{1}{2}}$ and $\Sigma^{-\frac{1}{2}}$ is often computationally expensive in practice. Instead, we employ an alternative least square approach (ALS) to update X and W

$$X = Y \Sigma^{-1} W (W^T \Sigma^{-1} W + \epsilon I)^{-1} \quad (35)$$

$$W = Y^T \Omega^{-1} X (X^T \Omega^{-1} X + \epsilon I)^{-1}, \quad (36)$$

where ϵ is a small positive constant to protect the inverse of matrices from singular.

Updating Ω and Σ : A straightforward approach is to optimize Ω and Σ iteratively as follows:

$$\begin{cases} \hat{\Omega} = \arg \min_{\Omega} \text{tr}(\Omega^{-1} S_1) + \log |\Omega| + \lambda_1 \|\Omega^{-1}\|_1 \\ \hat{\Sigma} = \arg \min_{\Sigma} \text{tr}(\Sigma^{-1} S_2) + \log |\Sigma| + \lambda_2 \|\Sigma^{-1}\|_1 \end{cases} \quad (37)$$

where

$$S_1 = \frac{1}{p} (Y - XW^T) \Sigma^{-1} (Y - XW^T)^T \quad (38)$$

$$S_2 = \frac{1}{n} (Y - XW^T)^T \Omega^{-1} (Y - XW^T) \quad (39)$$

We can regard S_1 and S_2 as the empirical covariances, and both problems in Eq. (37) are L_1 regularized precision matrix estimation, for which efficient optimization has been intensively studied (section 2.5). We adopt a fast and stable algorithm QUIC [41] for it as a basic solver:

$$\begin{cases} \hat{\Omega} = \text{QUIC}(S_1, \lambda_1) \\ \hat{\Sigma} = \text{QUIC}(S_2, \lambda_2) \end{cases} \quad (40)$$

The inference scheme is summarized in **Algorithm 1**. Given any invertible matrix P , $X P P^{-1} W^T$ equals $X W^T$. Therefore, X and W are not identifiable. To obtain a unique low-rank representation, we use GPCA [34] to post-process X and W . GPCA uses a generalized power method to obtain the columns of U and V sequentially. We note that Eq. (17) converges to the unique global solution when Ω^{-1} and Σ^{-1} are both positive-definite.

Algorithm 1 Maximum Regularized Likelihood

Input: data matrices Y , rank k

Output: X, W, Ω and Σ

- 1: Truncated k SVD of $Y = U_k \Sigma_k V_k^T$
 - 2: Initialize $X = U_k$ and $Y = \Sigma_k V_k^T$, $A = I$, $\Sigma = I$
 - 3: **repeat**
 - 4: update Ω
 - 5: update Σ
 - 6: **repeat**
 - 7: update X
 - 8: update W
 - 9: **until** convergence
 - 10: **until** Change of objective function value is small
-

3.4 Minimizing Wasserstein Distance

Though MRL is well-understood and relatively easy to implement, we still need to point out the following challenges. First, there are still too many parameters in the precision matrices, and the matrix decomposition procedure may collapse as it estimates two precision matrices Ω^{-1} and Σ^{-1} simultaneously. Second, the quadratic operator results in a block-concave problem with many local optima (strongly sensitive to initial starting solutions). Third, the regularized log-likelihood function has many local maximums, especially when the number of parameters is large. The first two challenges are the intrinsic problems produced by the way to model the data. In the following, we aim to solve the third challenge by minimizing the discrepancy between the white matrix normal distribution and that of the residue instead of maximizing the likelihood function.

First, recall the original model:

$$Y \sim \mathcal{MN}_{n,p}(M, \Omega, \Sigma), \quad (41)$$

if and only if

$$QYR \sim \mathcal{MN}_{n,p}(QMR, I, I), \quad (42)$$

where Q and R are both square, $Q^T Q = \Omega^{-1}$, $R^T R = \Sigma^{-1}$ and $M = XW^T$. It implies that the true factorization of Ω^{-1} and Σ^{-1} transform the residue matrix to IID gaussian noise. Then we transform the objective function by defining a divergence $D(\cdot|\cdot)$:

$$\min_{Q,R} D(Q(Y - M)R | \mathcal{MN}_{n,p}(0_{n \times p}, I_n, I_p)). \quad (43)$$

The choice of divergence is worthy of serious consideration. Note that our idea coincides with generative adversarial networks (GAN) [45]. GAN and its variants aim at minimizing the discrepancy between the true distribution and the generated distribution through a minimax game. The loss function (i.e., the divergence) to measure the discrepancy determines the quality of the generated samples. It plays an even more critical role in the GAN procedure than the structure of the neural networks of generator and discriminator. It is noticeable, however, that the target distribution of our model is the white multi-variate normal distribution, which is not as complicated as that of GAN. The method here is expected to be more accurate and stable.

The Kullback-Leibler (KL) divergence and its generalized version f -divergence may be the most commonly used ones. But they suffer from severe inaccuracy and instability due to their bad math property. When the two distributions

disjoint, the gradients vanish. The maximum mean discrepancy (MMD) performs well for matching high-dimensional standard normal distribution [46] and doesn't need a discriminator to enhance the stability. Note that in practice, we still need to sample from the normal distribution. And estimating MMD requires the size of samples is roughly proportional to the dimensionality of the input space. This lead to huge computation when the dimensionality is extremely high [47]. Besides, the effect of MMD depends on the kernel we choose. We cannot expect a kernel that abstracts all the characters of a distribution.

Instead of the KL and MMD divergences, we adopt the Wasserstein metric to measure the distance between two distributions. The Wasserstein metric is a true distance and has finer topology, which leads to effective gradients during optimization. However, computing the Wasserstein distance involves solving an optimal transportation problem, which is nontrivial. Its objective function can be written as:

$$\inf_{\pi \in \Pi(P_x, P_y)} \mathbb{E}_{(x,y) \sim \pi} [\|x - y\|_p] \quad (44)$$

where $\Pi(P_x, P_y)$ denotes the set of all joint distributions $\pi(x, y)$, whose marginals are respectively P_x and P_y . However, the infimum is highly intractable. Luckily, the Kantorovich-Rubinstein duality [48] holds when $p = 1$:

$$W_1(P_x, P_y) = \sup_{\|f\|_L \leq 1} \mathbb{E}_{s \sim P_x} [f(s)] - \mathbb{E}_{s \sim P_y} [f(s)] \quad (45)$$

which leads to a problem of approximating the optimal potential function f .

In practice, the neural network is often used to approximate the best f . It is easier to impose the 1-Lipschitz restriction on the function f with two main approaches: (1) clip the parameters of f to make it K -Lipschitz for some constant K [49]; (2) add a penalty term to enforce the gradient of f to be no more than 1 [50]. Based on these approaches, the Wasserstein-GAN works well and generates high-quality pictures. However, we still can not avoid the instability of GAN. Luckily, as the target distribution is the normal distribution, we have a direct solution to approximate the Wasserstein distance. Given the two normal distributions $x = \mathcal{N}(m_1, \Sigma_1)$ and $y = \mathcal{N}(m_2, \Sigma_2)$ with the means $m_{1,2} \in R^p$ and the covariance $C_{1,2} \in R^{p \times p}$, their squared Wasserstein distance is defined as [51]:

$$W(x, y)_2^2 = \|m_1 - m_2\|_2^2 + \text{tr}(\Sigma_1 + \Sigma_2 - 2(\Sigma_1^{\frac{1}{2}} \Sigma_2 \Sigma_1^{\frac{1}{2}})^{\frac{1}{2}}) \quad (46)$$

We use E to denote the current residue, i.e. $E = Y - M$, \tilde{E} to denote QER , σ^2 to denote the variance of noise. To pursue sparsity, we introduce the l_1 regularization as before. Note that the expectation of mean of E is zero, so we omit the computation of mean for both the norm and covariance in Eq. (46). When we update Q , the estimation of covariance among rows should be:

$$\Sigma = \frac{1}{p} \tilde{E} \tilde{E}^T, \quad (47)$$

then the objective function turns to:

$$\min_Q \text{tr}(\Sigma - 2\sigma\Sigma^{\frac{1}{2}}) + \lambda_1 \|Q^T Q\|_1 \quad (48)$$

The formula can be simpler since

$$\text{tr}(\Sigma) = \frac{1}{p} \text{tr}(\tilde{E}\tilde{E}^T) = \frac{1}{p} = \frac{1}{p} \|\tilde{E}\tilde{E}^T\|_2^2 \quad (49)$$

and

$$\text{tr}(\Sigma^{\frac{1}{2}}) = \frac{1}{\sqrt{p}} \text{tr}(\tilde{E}\tilde{E}^T)^{\frac{1}{2}} = \frac{1}{\sqrt{p}} \|\tilde{E}\|_*. \quad (50)$$

Hence, the objective function to update Q takes the form:

$$\min_Q \frac{1}{p} \|QER\|_2^2 - \frac{2\sigma}{\sqrt{p}} \|QER\|_* + \lambda_1 \|Q^T Q\|_1 \quad (51)$$

Similarly, the objective function for R is:

$$\min_R \frac{1}{n} \|QER\|_2^2 - \frac{2\sigma}{\sqrt{n}} \|QER\|_* + \lambda_2 \|R^T R\|_1. \quad (52)$$

Notice that the ratio of coefficients of $\|QER\|_2^2$ and $\|QER\|_*$ in the two objective functions Eq. (51) and Eq. (52) is different. When $n \neq p$, this can result in non-convergence. To address this issue, we balance the two functions by optimize:

$$\min_{Q,R} \frac{1}{\sqrt{np}} \|QER\|_2^2 - \frac{2}{\sqrt[4]{np}} \|QER\|_* + \lambda_1 \|Q^T Q\|_1 + \lambda_2 \|R^T R\|_1. \quad (53)$$

Not that if

$$Q^*, R^* = \arg \min_{Q,R} \frac{1}{\sqrt{np}} \|QER\|_2^2 - \frac{2}{\sqrt[4]{np}} \|QER\|_*, \quad (54)$$

then

$$\sqrt{\sigma} Q^*, \sqrt{\sigma} R^* = \arg \min_{Q,R} \frac{1}{\sqrt{np}} \|QER\|_2^2 - \frac{2\sigma}{\sqrt[4]{np}} \|QER\|_*. \quad (55)$$

Thus, there is no need to adjust the parameter σ . In the experiments, we find that the optimizing process converges faster with smaller σ . To keep the balance between Q and R , we normalize Q after each iteration, i.e., the average eigenvalues of Q and R are equal. Besides, the first term of the relaxed objective function (Eq. 53) is quadratic to Q and R , which can be solved efficiently. We implement the algorithm by using a gradient descent based optimization method in PyTorch.

Note that during the optimization, the distributions of columns and rows of residue are supposed to be multivariate normal rather than matrix normal in the original model. We have two explanations to argue in favor of it. First, since PCA assumes the distribution of noise follows IID Gaussian, the residue of each iteration should be mild, at least not sparse. Therefore, the first two order of moments can capture the real distribution. Second, we optimize the function through iterations. Though the approximation may not be accurate enough in the first few iterations, it has the ability of self-adaption and produces a good result.

3.5 Computational Complexity

Here we briefly discuss the computational complexity of maximum the regularized likelihood. At each iteration of updating X , the computational cost arises in matrix multiplication and inverse, which is $O(np^2 + r^3)$. Similarly, the computational cost for updating X is $O(n^2p + r^3)$.

Algorithm 2 MNPCA-W2

Input: data matrices Y , rank k , λ_1, λ_2

Output: X, Q and R

- 1: **repeat**
 - 2: Truncated k SVD of $X = SVD_k(QYR)$
 set $E = Y - Q^{-1}XR^{-1}$
 - 4: update Q and R by gradient descending:
 $\frac{1}{\sqrt{np}} \|QER\|_2^2 - \frac{2\sigma}{\sqrt[4]{np}} \|QER\|_*$
 - 6: **until** convergence
-

Solving Ω^{-1} and Σ^{-1} is much more computationally expensive. The dominant computational cost of QUIC is using the Cholesky decomposition at each iteration for the linear search of the step size to ensure the precision matrix is positive-definiteness. The the complexity of the Cholesky decomposition is $O(n^3)$ for updating Ω^{-1} ($O(p^3)$ for updating Σ^{-1}). Therefore, updating Ω^{-1} and Σ^{-1} can be very time-consuming. To address this problem, QUIC decomposes the precision matrix into smaller blocks with connected components and then runs the Cholesky decomposition for each blocks. For example, if Ω^{-1} consists of C connected components of size n_1, \dots, n_C ($n_1 + \dots n_C = n$). Then the time complexity of the Cholesky decomposition is reduced to $O(\max(\{n_i\}_{i=1, \dots, C}))$. The connected components of Ω^{-1} can be detected in $O(\|\Omega^{-1}\|_0)$, which is very efficient when Ω^{-1} is sparse (the situation of Σ^{-1} is the same). Empirically, the computational cost is affordable with sufficient large λ_1 and λ_2 when $\max(n, p) < 10^4$.

3.6 Tuning Parameters Selection

Given the desired dimension r , we should select the tuning parameters λ_1 and λ_2 to balance the trade-off of the log-likelihood value and the sparseness of the inferred precision matrices. While carrying a 2D grid search of λ_1 and λ_2 is computational expensive, we select λ_1 and λ_2 separately. Specifically, we use the Bayesian Information Criterion (BIC) to select appropriate λ_1 . The BIC for the L_1 -regularized precision matrix for a fixed value of λ_1 is given in [38]

$$\text{BIC}(\lambda_1) = -\log |\Omega^{-1}(\lambda_1)| + \text{tr}(S_1 \Omega^{-1}(\lambda_1)) + t_1 \frac{\log p}{p}, \quad (56)$$

where $\Omega^{-1}(\lambda_1)$ is inferred by Eq. (40). X and W are given by truncated r SVD and $\Sigma^{-1} = I$. t_1 is the number of non-zero entries in the upper diagonal portion of $\Omega^{-1}(\lambda_1)$.

To obtain a grid of values of λ_1 , we use the heuristic approach proposed in [52]. The largest value of the candidate λ_1 depends on the value of the empirical covariance

$$\lambda_{\max} = \max(\max(S_1 - I)_{ij} - \min(S_1 - I)_{ij})_{ij}. \quad (57)$$

We set $\lambda_{\min} = 0.1\lambda_{\max}$ and the candidate tuning parameters are ten values logarithmically spaced between λ_{\min} and λ_{\max} . The value of λ_1 minimizing the BIC is chosen as the final tuning parameter. We use the same procedure to choose λ_2 . There is lack of appropriate criterion to choose λ_1 parameter for MN-PCA-w2. We empirically set $\lambda_1 = \lambda_2 = 0.05$ in all the experiments.

4 EXPERIMENTAL RESULTS

In this section, we demonstrate the effectiveness of the proposed methods on both synthetic data and real-world data.

We first compare MN-PCA and PCA on both small-scale and large-scale synthetic data sets and then apply MN-PCA to non-linear synthetic data. We further conduct extensive experiments on various real-world data. All experiments are performed on a desktop computer with a 2GHz Intel Xeon E5-2683v3 CPU, a GTX 1080 GPU card and 16GB memory.

4.1 Synthetic Experiments

4.1.1 Small-Scale Synthetic Data

We construct the toy data with $Y = M + E$, where $Y \in R^{n \times p}$ is the observed data matrix, M is the low-rank signal and E is the matrix normal noise. Each row of M are drawn from r different centroids which are row vectors of length p . We then add the matrix normal noise $E \sim \mathcal{MN}(0, \Omega, \Sigma)$ to M . As we assume the precision matrices Ω^{-1} and Σ^{-1} are sparse, we generate a symmetric definite sparse matrix Ω^{-1} with sparsity parameter α_1 and condition number c_1 . Similarly, we generate Σ^{-1} with parameters α_2 and c_2 . We always set $c_1 = c_2 = c$, $\alpha_1 = \alpha_2 = \alpha$ for simplicity in the following experiments. Note that $c = 1$ and $\alpha = 0$ correspond to the IID situation.

We generate data with $n = 300$, $p = 200$, $r = 2$, $\alpha = 10^{-2}$. M consists of 300 samples drawn evenly from three different centroids. Specifically, the first and last 20 entries of centroid 1 equal one; the first and last 20 entries of centroid 2 equal minus one; the first 20 entries of centroid 3 equal one and the last 20 entries equal minus one. To investigate the effects of the graphical noise, we vary the condition number c from 8 to 224. We generate 10 synthetic data for each parameter combination. The l_1 penalty parameters λ_1, λ_2 of maximum the likelihood are selected by the aforementioned procedure.

We investigate the effect of graphical noise on the performance of PCA and the proposed methods measured in terms of low-rank matrix recovery (Table 1). Specifically, let the estimated low-rank matrix be \hat{M} , and the true low-rank matrix be M^* . We calculate the root mean square root (RMSE) by $\|\hat{M} - M^*\|_F / \sqrt{np}$ and peak signal to noise ratio (PSNR), respectively. We also apply K-means clustering to the projected data and compute the normalized mutual information (NMI) to evaluate the low-rank recovery implicitly. Both proposed methods outperform PCA in terms of all computed metrics. PCA works well when $c = 8$ because the distribution of the noise is close to IID normal distribution when c is small. The performance of the three methods decreases as the condition numbers increase. The maximum likelihood method becomes unstable along with the increase of the condition numbers. On the other hand, MN-PCA-w2 is more robust and outperforms MN-PCA when the condition number is sufficiently large.

We compare the performance of the proposed methods with QUIC in terms of the precision matrices estimation (Table 2). To facilitate the comparison, we apply QUIC to among-row and among-column covariance, respectively. Since there are many small values in the true precision matrices, we only treat the top 150 non-diagonal entries as non-zero values (by absolute value). We summarize the

performance in terms of true positive rate, true negative rate, and predictive positive value, defined as follows:

$$\text{TPR} = \frac{\#\{\hat{\Omega}_{ij} \neq 0 \& \Omega_{ij} \neq 0\}}{\#\{\Omega_{ij} \neq 0\}}, \text{TNR} = \frac{\#\{\hat{\Omega}_{ij} = 0 \& \Omega_{ij} = 0\}}{\#\{\Omega_{ij} = 0\}} \quad (58)$$

and

$$\text{PPV} = \frac{\#\{\hat{\Omega}_{ij} \neq 0 \& \Omega_{ij} \neq 0\}}{\#\{\hat{\Omega}_{ij} \neq 0\}}. \quad (59)$$

Numerical results from Table 2 reveal some interesting conclusions. 1) MN-PCA outperforms QUIC and MN-PCA-w2. 2) The TPR of all methods is relatively low. It is difficult to recover all non-zero entries in the true precision matrices of the noise as there may exist many small values. 3) The TNR of all methods is close to one. The BIC criterion is prone to choose sparser models, as discussed in [42], [52]. 4) It is not surprising that QUIC has lower TPR due to the existence of the low-rank matrix. But the TPR of QUIC increases along with the increase of the condition numbers. It is easier for QUIC to find true interactions when the effect of the matrix normal noise is stronger. 5) On the other hand, the TPR of the proposed methods increases first and then decreases with the condition numbers increase. When the effect of the matrix normal noise is small, it is difficult to capture the structure of the precision matrices. However, if the effect of the noise is too strong, the estimated low-rank matrix may mislead us in the inference of the precision matrices. 6) The PPV of MN-PCA is significantly higher than that of QUIC. Therefore, the FDR ($\text{FDR} = 1 - \text{PPV}$) of the proposed methods is acceptable when the condition number is mild. MN-PCA may help scientists to discover the underlying statistical correlations in the noise, which are ignored by PCA and most of its variants.

We illustrate the difference between MN-PCA and PCA on data generated with mild and large c , respectively (Fig. 3). We can see that both MN-PCA and MN-PCA-w2 have clear clusters when the condition number is mild ($c = 32$). The bottom row shows that when the condition number is large ($c = 224$), PCA has inferior performance. The projection of MN-PCA is more dispersed than that of MN-PCA-w2, suggesting that minimizing the Wasserstein distance is more accurate when the condition number is large.

4.1.2 Large-Scale Synthetic Data

To investigate the performance of the proposed methods on large-scale data, we construct a set of synthetic data with a similar strategy. We generate data with $n = 1000$, $r = 2$, $c = 196$, $\alpha_1 = 10^{-2}$, $\alpha_2 = 10^{-3}$ and vary p from 2000 to 6000. The first 10% features of centroid 1 equal one; the last 10% features of centroid 2 equal one; the first 10% features of centroid 3 equal one and the last 10% features equal minus one. The results are the average of 5 runs.

We also show the performance of low-rank recovery on the large-scale synthetic data (Table 3). PCA fails to produce meaningful projection for that the NMI is close to zero. MN-PCA-w2 significantly outperforms MN-PCA in terms of PSNR and RMSE. But MN-PCA has a better performance in clustering than that of MN-PCA-w2. It suggests that MN-PCA-w2 tends to recover the low-rank matrix more accurately, but the projection of MN-PCA is more dispersed and thus may have a better performance in clustering.

TABLE 1
Performance of low-rank recovery on Small Synthetic Datasets

	PSNR			RMSE			NMI		
	PCA	MN-PCA	MN-PCA-w2	PCA	MN-PCA	MN-PCA-w2	PCA	MN-PCA	MN-PCA-w2
$c = 8$	15.71(0.24)	16.79(0.19)	16.64(0.17)	0.16(0.00)	0.14(0.00)	0.15(0.00)	98.93(1.26)	99.31(0.89)	98.22(1.69)
$c = 16$	14.15(0.72)	16.34(0.28)	16.28(0.23)	0.20(0.02)	0.15(0.00)	0.15(0.00)	98.19(1.93)	99.29(0.91)	99.30(0.90)
$c = 32$	9.21(1.48)	15.64(0.36)	13.12(3.55)	0.35(0.05)	0.17(0.01)	0.24(0.10)	73.87(12.75)	97.94(1.75)	82.88(18.82)
$c = 64$	5.62(1.24)	11.07(4.16)	11.36(3.34)	0.53(0.08)	0.31(0.15)	0.29(0.10)	40.33(12.43)	70.00(34.42)	75.40(19.51)
$c = 96$	3.09(1.49)	6.94(3.71)	10.37(3.02)	0.71(0.12)	0.48(0.15)	0.32(0.09)	17.89(14.10)	43.42(36.95)	70.16(18.95)
$c = 128$	1.52(1.24)	4.32(1.09)	9.58(3.40)	0.85(0.12)	0.61(0.07)	0.35(0.12)	7.33(6.33)	25.62(27.49)	58.78(34.88)
$c = 160$	0.43(1.14)	2.83(1.92)	9.33(3.19)	0.96(0.13)	0.74(0.17)	0.36(0.12)	3.68(2.21)	18.13(25.01)	59.25(34.74)
$c = 192$	-0.42(1.18)	1.78(1.94)	9.62(3.24)	1.06(0.14)	0.83(0.19)	0.35(0.14)	2.68(1.41)	17.39(25.24)	68.71(28.93)
$c = 224$	-1.14(1.24)	0.54(1.80)	8.99(3.28)	1.15(0.16)	0.96(0.20)	0.38(0.14)	2.08(1.07)	13.00(19.45)	63.86(27.14)

The best performances are shown in bold.

TABLE 2
Performance of precision matrix estimation on Small Synthetic Datasets

	TPR ₁			TNR ₁			PPV ₁		
	QUIC	MN-PCA	MN-PCA-w2	QUIC	MN-PCA	MN-PCA-w2	QUIC	MN-PCA	MN-PCA-w2
$c = 8$	0.17(0.05)	0.35(0.08)	0.12(0.03)	1.00(0.00)	1.00(0.00)	1.00(0.00)	0.58(0.12)	0.75(0.12)	0.19(0.04)
$c = 16$	0.21(0.06)	0.45(0.11)	0.18(0.03)	1.00(0.00)	1.00(0.00)	1.00(0.00)	0.33(0.08)	0.73(0.16)	0.26(0.04)
$c = 32$	0.25(0.06)	0.45(0.10)	0.22(0.04)	1.00(0.00)	1.00(0.00)	1.00(0.00)	0.33(0.05)	0.80(0.15)	0.31(0.03)
$c = 64$	0.27(0.05)	0.38(0.09)	0.26(0.03)	1.00(0.00)	1.00(0.00)	1.00(0.00)	0.34(0.05)	0.83(0.13)	0.34(0.03)
$c = 96$	0.28(0.05)	0.39(0.09)	0.29(0.03)	1.00(0.00)	1.00(0.00)	1.00(0.00)	0.35(0.05)	0.72(0.18)	0.37(0.03)
$c = 128$	0.30(0.05)	0.38(0.10)	0.30(0.03)	1.00(0.00)	1.00(0.00)	1.00(0.00)	0.37(0.04)	0.75(0.16)	0.38(0.02)
$c = 160$	0.29(0.05)	0.34(0.09)	0.32(0.04)	1.00(0.00)	1.00(0.00)	1.00(0.00)	0.37(0.04)	0.78(0.15)	0.39(0.03)
$c = 192$	0.31(0.05)	0.33(0.09)	0.32(0.04)	1.00(0.00)	1.00(0.00)	1.00(0.00)	0.38(0.04)	0.76(0.16)	0.39(0.03)
$c = 224$	0.30(0.06)	0.31(0.09)	0.32(0.04)	1.00(0.00)	1.00(0.00)	1.00(0.00)	0.38(0.05)	0.74(0.17)	0.39(0.03)

	TPR ₂			TNR ₂			PPV ₂		
	QUIC	MN-PCA	MN-PCA-w2	QUIC	MN-PCA	MN-PCA-w2	QUIC	MN-PCA	MN-PCA-w2
$c = 8$	0.09(0.02)	0.22(0.05)	0.17(0.03)	0.99(0.00)	1.00(0.00)	0.99(0.00)	0.12(0.03)	0.94(0.05)	0.20(0.02)
$c = 16$	0.11(0.03)	0.30(0.06)	0.21(0.05)	0.99(0.00)	1.00(0.00)	0.99(0.00)	0.14(0.03)	0.84(0.10)	0.24(0.04)
$c = 32$	0.13(0.03)	0.28(0.07)	0.24(0.05)	0.99(0.00)	1.00(0.00)	0.99(0.00)	0.16(0.03)	0.84(0.11)	0.26(0.03)
$c = 64$	0.14(0.03)	0.19(0.06)	0.26(0.06)	0.99(0.00)	1.00(0.00)	0.99(0.00)	0.18(0.03)	0.82(0.13)	0.28(0.04)
$c = 96$	0.15(0.03)	0.22(0.06)	0.28(0.08)	0.99(0.00)	1.00(0.00)	0.99(0.00)	0.18(0.03)	0.65(0.14)	0.29(0.05)
$c = 128$	0.15(0.03)	0.19(0.05)	0.28(0.07)	0.99(0.00)	1.00(0.00)	0.99(0.00)	0.18(0.03)	0.68(0.14)	0.28(0.05)
$c = 160$	0.15(0.03)	0.16(0.05)	0.28(0.08)	0.99(0.00)	1.00(0.00)	0.99(0.00)	0.18(0.03)	0.70(0.13)	0.28(0.05)
$c = 192$	0.14(0.04)	0.16(0.04)	0.30(0.07)	0.99(0.00)	1.00(0.00)	0.99(0.00)	0.18(0.04)	0.72(0.16)	0.30(0.05)
$c = 224$	0.15(0.03)	0.14(0.05)	0.30(0.07)	0.99(0.00)	1.00(0.00)	0.99(0.00)	0.18(0.03)	0.65(0.16)	0.30(0.05)

TPR₁, TNR₁, PPV₁ denote true positive rate, true negative rate and positive predictive value of estimated Ω^{-1} , respectively. TPR₂, TNR₂, PPV₂ denote the corresponding metrics of estimated Σ^{-1} , respectively.

We also show the running time of MN-PCA and MN-PCA-w2 (Fig. 4). MN-PCA is much faster than MN-PCA-w2. We further investigate the relationship between l_1 regularization parameter and running time. We fix λ_1 and vary λ_2 linearly in the logarithmic space. The running time of MN-PCA drops down rapidly with the increase of λ_2 . A large l_1 parameter encourages the sparsity of the estimated precision matrix, allowing us to use the Cholesky decomposition on each block. The running time of MN-PCA-w2 almost does not change in terms of λ_2 since its inference is based on gradient descent.

4.1.3 Swiss Roll Data

We then compare our algorithms with PCA on the Swiss roll data. Swiss roll data is widely used to test out various dimensionality reduction algorithms. The idea of Swiss roll data is to create several points in 2D space and then map them to 3-D space. Algorithms considering the local geometry structure can unfold the roll successfully to 2D space, such as isomap [53], LLE [54] and SDE [55].

We create two rolls, as shown in the first panel of Fig. 5 and then use PCA and the proposed methods to project the

data points to 2D space. Fig. 5 presents that the two clusters in the projection of PCA are mixed. But we can identify those two clusters from the projection of the proposed methods. Note we don't consider the local geometry or geodesic distance explicitly. Therefore, our methods don't preserve the local geometry structure of high-dimensional space. But the precision matrix somehow reflects the local structure and may guide us to obtain a better representation.

4.2 Real-World Experiments

In this section, we show the effectiveness of MN-PCA and compare it with PCA as well as three other competing methods on various real-world data. **Kernel PCA** is an extension of PCA, and it adopts the kernel idea to handle nonlinear data. However, how to choose an appropriate kernel for the given data is still unknown. Therefore, we apply three different kernels (i.e., linear, Gaussian, and polynomial) with recommended parameters to the data. **ICA** has been well studied and extensively used in signal processing. We use an efficient and popular algorithm FastICA proposed by [56] for comparison. **GPCA** is the most competing approach [34].

TABLE 3
Performance of low-rank recovery on Large Synthetic Datasets

	PSNR			RMSE			NMI		
	PCA	MN-PCA	MN-PCA-w2	PCA	MN-PCA	MN-PCA-w2	PCA	MN-PCA	MN-PCA-w2
$p = 2000$	4.53(0.50)	20.06(1.19)	20.99(0.17)	0.59(0.03)	0.10(0.01)	0.09(0.00)	4.32(7.86)	98.80(1.18)	96.70(2.17)
$p = 3000$	4.79(0.46)	7.49(0.65)	20.59(0.23)	0.58(0.03)	0.42(0.03)	0.09(0.00)	4.88(7.34)	85.13(9.73)	96.75(1.80)
$p = 4000$	4.10(0.51)	12.51(5.74)	14.96(0.97)	0.62(0.04)	0.28(0.17)	0.18(0.02)	0.83(0.09)	90.75(11.66)	73.47(7.52)
$p = 5000$	4.47(0.25)	7.76(0.38)	10.87(0.22)	0.60(0.02)	0.41(0.02)	0.29(0.01)	1.42(0.44)	82.98(11.91)	47.62(1.57)
$p = 6000$	3.71(0.66)	5.60(2.30)	10.69(0.20)	0.65(0.05)	0.54(0.14)	0.29(0.01)	1.57(0.53)	59.43(32.38)	44.40(1.65)

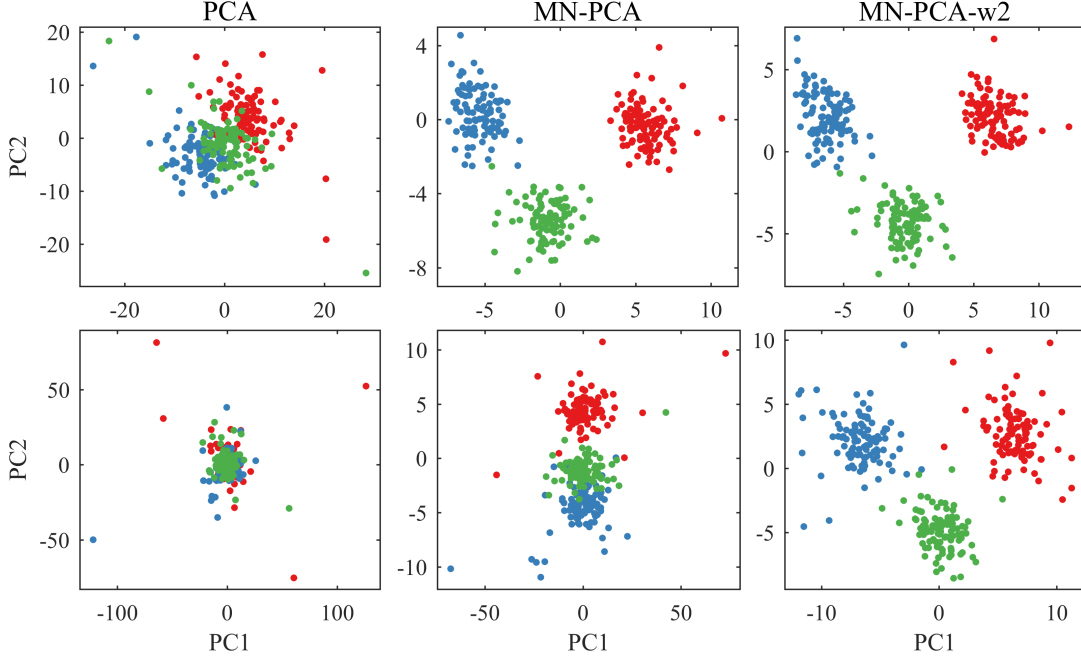


Fig. 3. Illustration of PCA, MN-PCA and MN-PCA-w2 on small synthetic data. Top: $c = 32$. Bottom: $c = 224$.

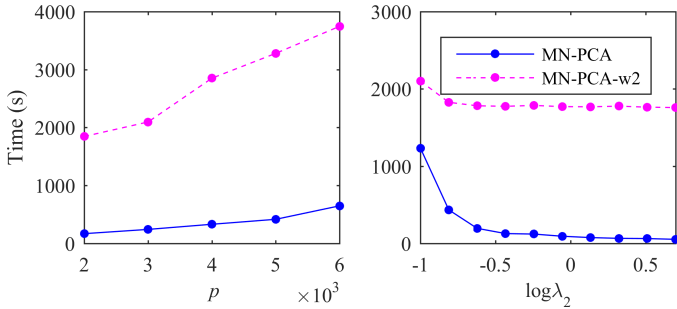


Fig. 4. Running time of MN-PCA and MN-PCA-w2 on synthetic data of $n = 1000$, $c = 192$. Left: time versus data size. Right: time versus logarithm of l_1 regularization parameter λ_2 with $p = 2000$.

However, it requires the precision matrix Ω^{-1} and Σ^{-1} to be predefined. Two empirical ways have been suggested to set it: 1) the inverse smoothing matrix, which is computed by the Laplacian matrix L ; 2) the standard exponential smoothing matrix S , which is based on the distance matrix. Finally, there are four different settings for GPCA, denoted as LL, LS, SL, and SS, respectively.

The statistics of the 14 datasets used for evaluation are summarized in Table 4. More details are described in the

Supplementary Materials.

TABLE 4
Summary of the Datasets

Datasets	# Samples(n)	# Features(p)	# Classes
balance-scale	625	4	3
german	1000	20	2
glass	214	9	6
heart-statlog	270	13	2
iono	351	34	2
sonar	208	60	2
tae	151	5	3
vehicle	846	18	4
wine	178	13	3
wisc	699	9	2
zoo	101	16	7
METABRIC	1975	1000	5
gse29505	290	384	2
3sources	352	700	6

The MN-PCA, as well as other compared methods, requires an approximation of the rank of the data matrix. We adopt the bi-cross validation method, which is proposed by [57] and is also used in [58]. Specifically, we first approximate the data matrix by the truncated SVD \hat{Y}_k where $\hat{Y}_k = \sum_{j=1}^k \hat{d}_j \hat{u}_j \hat{v}_j^T$. The proportion of variance explained is defined as $R_i = \sum_{j=1}^i \hat{d}_j^2 / \sum_{j=1}^k \hat{d}_j^2$. Note that

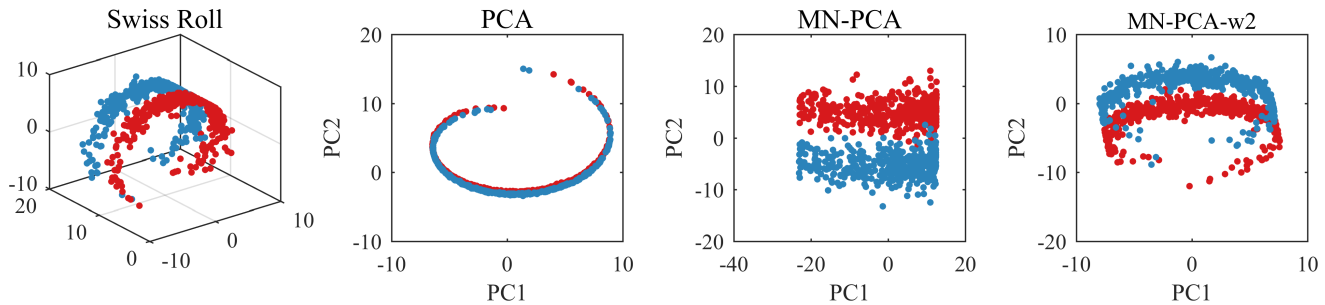


Fig. 5. Illustration of PCA and MN-PCA on Swiss roll data. From left to right: the 3-D scatter plot of Swiss roll data; the projection of PCA; the projection of MN-PCA; the projection of MN-PCA-w2

R_i is between 0 and 1 and grows with i . We assume that the redundant components should not contribute much to the total variance. The final rank estimation is the smallest integer r which satisfies $R_r > \tau$ where $\tau > 0$ is the thresholding proportion value (e.g. 0.8) and $1 \leq r \leq k$.

In the following experiments, we set $k = 10$ and $\tau = 0.8$ to choose the rank for dimension reduction. If the number of features are smaller than 15, we simply set $r = 2$. Then we use a Least-squares SVM (LSSVM) [59] with a Gaussian kernel as a benchmark classifier to evaluate the quality of the low-rank presentation. To facilitate a fair comparison, we choose the hyperparameter of LSSVM by 5-fold cross validation. The accuracy is the average of 10 runs.

We demonstrate the experimental performance of these methods on the 14 real-world datasets (Table 5). We could clearly find the following observations. 1) Our methods have competitive or superior performance compared with PCA in most cases, suggesting that MN-PCA could obtain more informative representation in some real applications. 2) The performance of GPCA is poorer than MN-PCA in general. Although GPCA with the predefined precision matrices was considered to work well on the brain MRI data, it needs to choose appropriate precision matrices in advance, which is not suitable for general data. 3) The performance of GPLVM is similar to PCA. 4) The performance of KPCA with different kernels are very different. 5) Both KPCA and GPLVM adopt the kernel trick to handle the nonlinear data, but it is challenging to choose an appropriate kernel for a given data. 6) ICA sometimes produces inferior performance. A possible reason is that the non-Gaussian assumption of ICA is too restrictive.

4.3 The Estimated Precision Matrix is Informative

We have shown the effectiveness of MN-PCA in terms of dimension reduction and low-rank representation. Furthermore, numerical results show that the estimated precision matrices reveal some inspiring patterns in the noise. For example, we take the METABRIC data as an illustrating example. It contains a large cohort of around 2000 breast cancer patients with detailed clinical measurements and genome-wide molecular profiles. How to use the gene expression profile to classify invasive breast cancer into biologically and clinically distinct subtypes has been intensively studied. Here, we use the famous PAM50 subtypes as the reference [60] to evaluate the low-rank representation and graphical noise structure. We select the top 1000 genes by

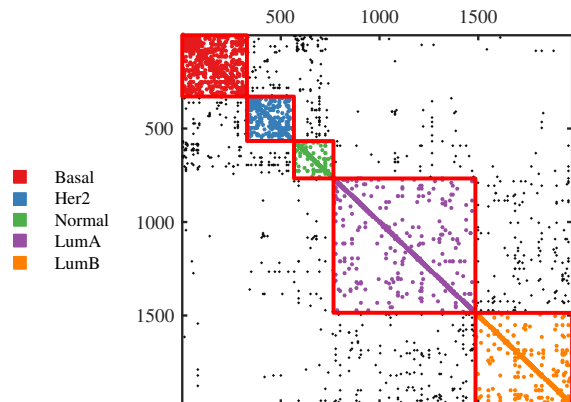


Fig. 6. Illustration of the estimated precision matrix of MN-PCA in the sample space. It is reordered based on the subtypes with $k = 5$. Since the estimated precision matrix contains many small values which should be less significant, only top 1000 interactions are shown.

coefficients of variation and focus on the precision matrix in the sample space. The estimated rank $r = 5$. There are 5504 edges in the estimated precision matrix (Fig 6). It demonstrates that the interactions within subtypes tend to be denser than between subtypes, and biologically relevant subtypes have more interactions. For example, LumA and LumB have more interactions. Normal-like subtypes have many interactions with the other subtypes.

The next example is about 3Sources data, which is collected from three well-known online news sources, including BBC, Reuters, and The Guardian. Here we use the documents collected from the BBC as an example. The document term matrix is of size 352×3560 . We remove the terms that appear less than 20 times in documents. There are 700 terms left. We focus on the estimated precision matrix in the feature space, which reveals the relationship of terms in the documents. The estimated rank $r = 7$, and there are 651 edges. We note that the semantically related terms tend to have interactions. For example, the top 5 term (chosen by absolute values) pairs are "premier/league", "study/research", "executive/chief", "minister/primer", "journal/study", respectively. Those term pairs frequently appear in the same documents.

5 DISCUSSION AND CONCLUSION

In this paper, we propose MN-PCA to model the graphical noise in both the feature and sample spaces. MN-PCA can

TABLE 5
Performance of Dimension Reduction on Real-world Datasets

Dataset	PCA	GPLVM	KPCA (lin)	KPCA (gau)	ICA	GPCA (LS)	GPCA (SL)	MN-PCA	MN-PCA-w2
balance-scale	66.37(0.76)	68.05(0.74)	52.51(0.74)	63.34(0.34)	61.94(0.63)	-	-	77.39(1.11)	75.30(0.37)
german	71.02(0.65)	70.31(0.36)	71.05(0.74)	70.25(0.14)	72.71(0.60)	71.26(0.63)	-	71.48(0.65)	71.88(0.54)
glass	56.18(0.94)	56.32(1.39)	51.54(2.03)	32.14(1.91)	16.96(1.01)	-	-	61.01(2.18)	47.15(0.89)
heart-statlog	80.33(0.95)	82.96(0.65)	83.52(0.94)	74.11(1.79)	76.56(0.25)	74.56(1.16)	-	82.07(0.66)	82.70(0.72)
iono	93.16(0.67)	93.53(0.36)	92.99(0.57)	92.02(0.43)	89.86(0.61)	-	-	91.17(0.43)	92.09(0.67)
sonar	85.83(2.21)	71.16(2.49)	85.54(2.34)	59.09(3.35)	49.66(2.05)	85.44(1.32)	-	85.34(1.68)	81.15(2.15)
tae	43.13(4.47)	42.71(5.00)	40.71(2.77)	54.83(3.37)	46.49(3.22)	-	-	49.55(3.11)	42.43(4.35)
vehicle	45.72(0.64)	46.60(0.71)	43.83(0.89)	28.90(0.74)	9.79(0.58)	50.07(1.38)	-	51.72(0.93)	58.17(0.93)
wine	95.95(0.24)	95.79(0.60)	95.79(0.40)	90.93(1.25)	56.29(2.01)	63.82(1.72)	-	96.74(0.44)	93.09(0.28)
wisc	96.85(0.13)	96.81(0.14)	96.87(0.17)	95.95(0.14)	91.39(0.55)	-	-	96.50(0.24)	96.15(0.17)
zoo	89.51(1.25)	85.72(1.38)	87.50(1.95)	66.77(2.66)	73.77(3.26)	-	88.63(2.10)	76.45(4.61)	90.46(5.21)
metabric	66.12(0.28)	65.85(0.32)	67.08(0.32)	4.52(0.21)	1.58(0.24)	50.96(0.86)	62.49(0.46)	67.74(0.62)	61.25(0.34)
gse29505	92.86(0.56)	92.86(0.56)	92.59(0.55)	59.90(0.54)	48.97(3.25)	87.07(0.97)	95.76(0.73)	93.24(0.52)	92.31(0.61)
3sources	70.55(1.82)	69.89(0.99)	70.59(1.22)	2.47(0.46)	0.03(0.09)	-	14.26(1.31)	76.78(0.88)	63.15(1.26)

Top two of **clustering accuracy** are shown in bold. GPCA fails to produce results when the predefined precision matrices are ill-conditioned. Due to space limitations, we show the results of KPCA with polynomial kernel, GPCA(LL) and GPCA(SS) in the Supplementary Materials.

also be regarded as the minimization of the reconstruction error over the generalized Mahalaobis distance. Thus, PCA is a special case of it with the noise of identity covariance matrices. We develop two algorithms for inference: 1) Maximizing the regularized likelihood, which turns to be an iterative method. This algorithm works well on the synthetic data when the effect of the matrix normal noise is mild and can handle relatively large data. But it is not robust when the condition numbers get larger. To address this challenge, we propose 2) MN-PCA-w2, which aims at minimizing the Wasserstein distance between the distribution of the transformed residue and the distribution of white noise. The second algorithm is inspired by GAN and more robust when the effect of the matrix normal noise is large. However, it is inefficient for large datasets. We extensively compared the two algorithms on synthetic data. The experimental results on synthetic datasets also show that considering the structural noise brings an improvement in clustering performance and encourages to find better low-rank representation. The experimental results on real-world datasets show that the proposed methods are competitive or superior to the compared methods. It suggests the effectiveness of our methods. Moreover, the inferred precision matrices are also informative and may help us understand the underlying structure of the noise.

There are several questions that remain to be investigated. First, the inference of MN-PCA-w2 is inefficient for large data. The objective function involving the square root of the precision matrix makes it challenging to solve. As MN-PCA-w2 shows promising results on synthetic data, it is worth studying how to develop a more efficient and robust algorithm. Second, our proposed methods are not guaranteed to provide a better low-rank representation for clustering and classification. As we demonstrate in the real-world experiments, the estimated precision matrices are also informative. If the inferred structure of the noise captures the information related to clustering and classification, the performance of the low-rank representation possibly decreases. One crucial problem is that what is the noise, and what is the signal? Conventional methods such as PCA assume the noise is white noise, which is seldom satisfied.

In this paper, we model the graphical noise by matrix normal distribution. Although it is difficult to determine what information is captured in the estimated noise without external knowledge, our methods provide an approach for data exploration for users to obtain the low-rank representation and discover the underlying structure of the noise simultaneously.

REFERENCES

- [1] K. Pearson, "Liii. on lines and planes of closest fit to systems of points in space," *The London, Edinburgh, and Dublin Philosophical Magazine and Journal of Science*, vol. 2, no. 11, pp. 559–572, 1901.
- [2] B. Moore, "Principal component analysis in linear systems: controllability, observability, and model reduction," *IEEE Trans. Autom. Control*, vol. 26, no. 1, pp. 17–32, 1981.
- [3] P. J. Hancock, A. M. Burton, and V. Bruce, "Face processing: human perception and principal components analysis," *Memory & Cognition*, vol. 24, no. 1, pp. 26–40, 1996.
- [4] T. Hastie *et al.*, "Gene shaving as a method for identifying distinct sets of genes with similar expression patterns," *Genome Biology*, vol. 1, no. 2, p. research0003, 2000.
- [5] J. Wright, A. Ganesh, S. Rao, Y. Peng, and Y. Ma, "Robust principal component analysis: exact recovery of corrupted low-rank matrices via convex optimization," in *Advances in Neural Information Processing Systems*, 2009, pp. 2080–2088.
- [6] H. Xu, C. Caramanis, and S. Sanghavi, "Robust PCA via outlier pursuit," in *Advances in Neural Information Processing Systems*, 2010, pp. 2496–2504.
- [7] C. E. J. ès, X. Li, Y. Ma, and J. Wright, "Robust principal component analysis?" *J. ACM*, vol. 58, no. 3, p. 11, 2011.
- [8] Y. Peng, A. Ganesh, J. Wright, W. Xu, and Y. Ma, "Rasl: robust alignment by sparse and low-rank decomposition for linearly correlated images," *IEEE Trans. Pattern Anal. Mach. Intell.*, vol. 34, no. 11, pp. 2233–2246, 2012.
- [9] G. Liu, Z. Lin, S. Yan, J. Sun, Y. Yu, and Y. Ma, "Robust recovery of subspace structures by low-rank representation," *IEEE Trans. Pattern Anal. Mach. Intell.*, vol. 35, no. 1, pp. 171–184, 2013.
- [10] N. Shahid, V. Kalofolias, X. Bresson, M. Bronstein, V. and P. erghenst, "Robust principal component analysis on graphs," in *Proc. IEEE Int. Conf. Comput. Vision*, 2015, pp. 2812–2820.
- [11] S. Gao, I. W.-H. Tsang, L.-T. Chia, and P. Zhao, "Local features are not lonely - laplacian sparse coding for image classification," *Proc. Comput. Soc. Conf. Comput. Vision Pattern Recognit.*, 2010.
- [12] M. Zheng *et al.*, "Graph regularized sparse coding for image representation," *IEEE Trans. Image Process.*, vol. 20, no. 5, pp. 1327–1336, 2011.
- [13] M. Yin, J. Gao, Z. Lin, Q. Shi, and Y. Guo, "Dual graph regularized latent low-rank representation for subspace clustering," *IEEE Trans. Image Process.*, vol. 24, no. 12, pp. 4918–4933, 2015.

- [14] D. Cai, X. He, J. Han, and T. S. Huang, "Graph regularized nonnegative matrix factorization for data representation," *IEEE Trans. Pattern Anal. Mach. Intell.*, vol. 33, no. 8, pp. 1548–1560, 2011.
- [15] S. Zhang, Q. Li, J. Liu, and X. J. Zhou, "A novel computational framework for simultaneous integration of multiple types of genomic data to identify microRNA-gene regulatory modules," *Bioinformatics*, vol. 27, no. 13, pp. i401–i409, 2011.
- [16] M. E. Tipping and C. M. Bishop, "Probabilistic principal component analysis," *J. Royal Statistical Soc. B*, vol. 61, no. 3, pp. 611–622, 1999.
- [17] C. M. Bishop, "Bayesian PCA," in *Advances in Neural Information Processing Systems*, 1999, pp. 382–388.
- [18] J. Zhao and Q. Jiang, "Probabilistic PCA for t distributions," *Neurocomputing*, vol. 69, no. 16–18, pp. 2217–2226, 2006.
- [19] N. Wang, T. Yao, J. Wang, and D.-Y. Yeung, "A probabilistic approach to robust matrix factorization," in *Proc. Eur. Conf. Comput. Vision*. Springer, 2012, pp. 126–139.
- [20] J. Li and D. Tao, "Simple exponential family PCA," in *Proc. Int. Conf. Artif. Intell. and Statist.*, 2010, pp. 453–460.
- [21] C. Zhang and S. Zhang, "Bayesian joint matrix decomposition for data integration with heterogeneous noise," *IEEE Trans. Pattern Anal. Mach. Intell.*, pp. 1–1, 2019.
- [22] Q. Zhao, D. Meng, Z. Xu, W. Zuo, and L. Zhang, "Robust principal component analysis with complex noise," in *Proc. Int. Conf. Mach. Learn.*, 2014, pp. 55–63.
- [23] X. Cao *et al.*, "Low-rank matrix factorization under general mixture noise distributions," in *Proc. IEEE Int. Conf. Comput. Vision*, 2015.
- [24] A. A. Kalaitzis and N. D. Lawrence, "Residual component analysis: Generalising PCA for more flexible inference in linear-gaussian models," in *Proc. Int. Conf. Mach. Learn.* Omnipress, 2012, pp. 539–546.
- [25] S. Mika, B. Schölkopf, A. J. Smola, K.-R. Müller, M. Scholz, and G. Rätsch, "Kernel PCA and de-noising in feature spaces," in *Advances in Neural Information Processing Systems*, 1999, pp. 536–542.
- [26] C. Liu, "Gabor-based kernel PCA with fractional power polynomial models for face recognition," *IEEE Trans. Pattern Anal. Mach. Intell.*, vol. 26, no. 5, pp. 572–581, 2004.
- [27] N. Lawrence, "Probabilistic non-linear principal component analysis with gaussian process latent variable models," *J. Mach. Learn. Res.*, vol. 6, no. Nov, pp. 1783–1816, 2005.
- [28] C. M. Bishop and N. M. Nasrabadi, "Pattern recognition and machine learning," *J. Electronic Imag.*, vol. 16, p. 049901, 2007.
- [29] C. Eckart and G. Young, "The approximation of one matrix by another of lower rank," *Psychometrika*, vol. 1, no. 3, pp. 211–218, 1936.
- [30] T. Zhou and D. Tao, "Greedy bilateral sketch, completion & smoothing," in *Proc. Int. Conf. Artif. Intell. and Statist.*, 2013.
- [31] S. Ma and N. S. Aybat, "Efficient optimization algorithms for robust principal component analysis and its variants," *Proc. IEEE*, vol. 106, no. 8, pp. 1411–1426, 2018.
- [32] Y. Yankelevsky and M. Elad, "Dual graph regularized dictionary learning," *IEEE Trans. Signal Inf. Process. Netw.*, vol. 2, no. 4, pp. 611–624, 2016.
- [33] C. M. Bishop, "Variational principal components," in *Proc. Conf. Artif. Neural Netw.* IET, 1999.
- [34] G. I. Allen, L. Grosenick, and J. Taylor, "A generalized least-square matrix decomposition," *J. Amer. Statist. Assoc.*, vol. 109, no. 505, pp. 145–159, 2014.
- [35] M. E. Tipping, "Sparse kernel principal component analysis," in *Advances in Neural Information Processing Systems*, 2001, pp. 633–639.
- [36] B. Moghaddam, "Principal manifolds and probabilistic subspaces for visual recognition," *IEEE Trans. Pattern Anal. Mach. Intell.*, vol. 24, no. 6, pp. 780–788, 2002.
- [37] Z. Ge and Z. Song, "Kernel generalization of ppca for nonlinear probabilistic monitoring," *Industrial & Engineering Chemistry Research*, vol. 49, no. 22, pp. 11 832–11 836, 2010.
- [38] M. Yuan and Y. Lin, "Model selection and estimation in the gaussian graphical model," *Biometrika*, vol. 94, no. 1, pp. 19–35, 2007.
- [39] J. Friedman, T. Hastie, and R. Tibshirani, "Sparse inverse covariance estimation with the graphical lasso," *Biostatistics*, vol. 9, no. 3, pp. 432–441, 2008.
- [40] L. Li and K.-C. Toh, "An inexact interior point method for l1-regularized sparse covariance selection," *Math. Program. Computation*, vol. 2, no. 3–4, pp. 291–315, 2010.
- [41] C.-J. Hsieh, M. A. Sustik, I. S. Dhillon, and P. Ravikumar, "QUIC: quadratic approximation for sparse inverse covariance estimation," *J. Mach. Learn. Res.*, vol. 15, no. 1, pp. 2911–2947, 2014.
- [42] P. Danaher, P. Wang, and D. M. Witten, "The joint graphical lasso for inverse covariance estimation across multiple classes," *J. Royal Statistical Soc. B*, vol. 76, no. 2, pp. 373–397, 2014.
- [43] T. T. Cai, W. Liu, and H. H. Zhou, "Estimating sparse precision matrix: optimal rates of convergence and adaptive estimation," *Annal. Statist.*, vol. 44, no. 2, pp. 455–488, 2016.
- [44] J. Fan, Y. Liao, and H. Liu, "An overview of the estimation of large covariance and precision matrices," *The Econometrics Journal*, vol. 19, no. 1, pp. C1–C32, 2016.
- [45] I. Goodfellow *et al.*, "Generative adversarial nets," in *Advances in Neural Information Processing Systems*, 2014, pp. 2672–2680.
- [46] A. Gretton, K. M. Borgwardt, M. J. Rasch, B. Schölkopf, and A. Smola, "A kernel two-sample test," *J. Mach. Learn. Res.*, vol. 13, pp. 723–773, 2012.
- [47] S. Reddi, A. Ramdas, B. Póczos, A. Singh, and L. Wasserman, "On the high dimensional power of a linear-time two sample test under mean-shift alternatives," in *Proc. Int. Conf. Artif. Intell. and Statist.*, 2015, pp. 772–780.
- [48] C. Villani, *Optimal transport: old and new*. Springer Science & Business Media, 2008, vol. 338.
- [49] M. Arjovsky, S. Chintala, and L. Bottou, "Wasserstein GAN," *arXiv preprint arXiv:1701.07875*, 2017.
- [50] I. Gulrajani, F. Ahmed, M. Arjovsky, V. Dumoulin, and A. C. Courville, "Improved training of Wasserstein GANs," in *Advances in Neural Information Processing Systems*, 2017, pp. 5767–5777.
- [51] I. Olkin and F. Pukelsheim, "The distance between two random vectors with given dispersion matrices," *Linear Algebra and its Applications*, vol. 48, pp. 257–263, 1982.
- [52] T. Zhao, H. Liu, K. Roeder, J. Lafferty, and L. Wasserman, "The huge package for high-dimensional undirected graph estimation in R," *J. Mach. Learn. Res.*, vol. 13, pp. 1059–1062, 2012.
- [53] J. B. Tenenbaum, V. De Silva, and J. C. Langford, "A global geometric framework for nonlinear dimensionality reduction," *Science*, vol. 290, no. 5500, pp. 2319–2323, 2000.
- [54] S. T. Roweis and L. K. Saul, "Nonlinear dimensionality reduction by locally linear embedding," *Science*, vol. 290, no. 5500, pp. 2323–2326, 2000.
- [55] K. Q. Weinberger and L. K. Saul, "Unsupervised learning of image manifolds by semidefinite programming," *Int. J. Comput. Vision*, vol. 70, no. 1, pp. 77–90, 2006.
- [56] A. Hyvärinen and E. Oja, "Independent component analysis: algorithms and applications," *Neural Netw.*, vol. 13, no. 4–5, pp. 411–430, 2000.
- [57] A. B. Owen, P. O. Perry *et al.*, "Bi-cross-validation of the SVD and the nonnegative matrix factorization," *Annal. Statist.*, vol. 3, no. 2, pp. 564–594, 2009.
- [58] G. Chen, P. F. Sullivan, and M. R. Kosorok, "Biclustering with heterogeneous variance," *Proc. Natl. Acad. Sci. U.S.A.*, vol. 110, no. 30, pp. 12 253–12 258, 2013.
- [59] K. De Brabanter *et al.*, *LS-SVMlab toolbox user's guide: version 1.7*. Katholieke Universiteit Leuven, 2010.
- [60] J. S. Parker *et al.*, "Supervised risk predictor of breast cancer based on intrinsic subtypes," *J. Clin. Oncol.*, vol. 27, no. 8, p. 1160, 2009.